

Assuring safety of vision-based swarm formation control

Chiao Hsieh¹, Yangge Li¹, Yubin Koh¹ and Sayan Mitra¹

Abstract— Vision-based formation control systems recently have attracted attentions from both the research community and the industry for its applicability in GPS-denied environments. The safety assurance for such systems is challenging due to the lack of formal specifications for computer vision systems and the complex impact of imprecise estimations on distributed control. We propose a technique for safety assurance of vision-based formation control. Our technique combines (1) the construction of a piecewise approximation of the worst-case error of perception and (2) a classical Lyapunov-based safety analysis of the consensus control algorithm. The analysis provides the ultimate bound on the relative distance between drones. This ultimate bound can then be used to guarantee safe separation of all drones. We implement an instance of the vision-based control system on top of the photo-realistic AirSim simulator. We construct the piecewise approximation for varying perception error under different environments and weather conditions, and we are able to validate the safe separation provided by our analysis across the different weather conditions with AirSim simulation.

I. INTRODUCTION

The literature on distributed consensus, flocking, and formation control is vast (see, for example [1]–[4]). Flocking and swarm formation using computer vision [5]–[7] can leverage the advances in deep learning. They do not require localization systems, and thus, are attractive for GPS-denied environments. However, safety assurance of vision-based control systems poses challenges: (1) Formal specifications for computer vision systems are difficult, (2) deep learning-based perception functions can be fragile, and (3) safety analysis requires one to understand the impact of *imprecise* vision-based state (position) estimation on distributed control. These challenges have been recognized by the autonomy industry [8].

In this paper, we present a technique for safety assurance of a vision-based swarm formation control system. The computer vision pipeline here uses feature detection, feature matching across a pair of images, and geometric models for 3D-vision to estimate the pairwise relative poses of the participating drones. The estimated relative poses are then used by a consensus-based formation control algorithm to achieve target formations. To our knowledge, this is the first investigation of end-to-end safety assurance of such systems. Our technique combines (1) Lyapunov analysis of the formation control algorithm with (2) an *approximate abstraction* for the vision-based perception component. The notion of approximate abstraction was introduced in our prior work on vision-based lane keeping control [9]. The key idea



Fig. 1. Vision-based drone formation using downward facing camera images in AirSim.

was to approximate the worst case behavior of the complex perception system with a low-dimensional, and empirically precise, function of the ground truth lane-deviation values. Formation control for drones uses a completely different type of perception with pairs of images, feature matching, and camera geometry. Not surprisingly, a completely different method is needed for constructing the approximate abstraction. There are two key challenges are: (1) The perception error impacts the behavior agents in a distributed system. (2) The upper bound on the perception error for a pair of agents depends on their ground truth relative position. In general, perception errors can get worse as the system approaches the equilibrium (desired formation), and thus, make stabilization difficult. Asymptotic stability may be unachievable, and we have to settle for the more practical notion of ultimate boundedness [10]. Our analysis gives an empirical method for testing out the environmental conditions (e.g., lighting, fog) under which a target formation can be safely achieved, despite perception errors. Thus, this study shows that on top of the safety assurance, the methodology with approximate abstractions may be useful for creating safe operating guidelines for vision-based swarms.

In summary, our contributions are as follows: (1) An approach to construct a piecewise approximate abstraction to bound the perception error of the vision component. (2) A Lyapunov-based analysis to derive the ultimate bound for the end-to-end drone formation system using the approximate abstraction. (3) Detailed empirical evaluation of the approach with the photorealistic AirSim simulator [11]. Our implementation of vision-based formation control, and the code for simulation and analyses, are all publicly available¹.

¹The authors are with Coordinate Science Lab, University of Illinois Urbana-Champaign, Champaign, IL, USA {chsieh16, li213, yubink2, mitras}@illinois.edu

¹<https://gitlab.engr.illinois.edu/aap/airsim-vision-formation>

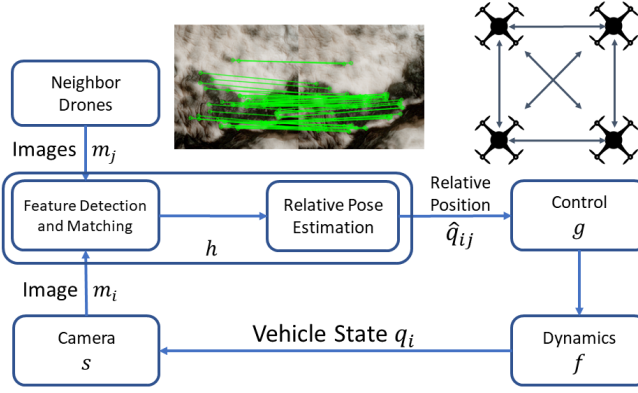


Fig. 2. Architecture of an agent in the vision-based formation control systems.

Related Works: There is a line of work on the analysis of closed-loop systems with vision-based perception. Our previous work [9] mentioned above provides the insight of approximate abstractions but focus on the lane tracking system. VerifAI [12] uses techniques like fuzz testing and simulation to falsify the system specifications. Katz et al. [13] trains generative adversarial networks (GANs) to produce a network to simplify the image-based NN. NNLander-VeriF [14] verifies NN perception along with NN controllers for an autonomous landing system. In contrast, this work is the first paper to provide safety analyses for a formation control system with vision-based perception, and we apply the notion of ultimate boundedness for safe separation and formation.

Paper Organization: In Section II, we introduce the formation control system with the vision-based perception. We briefly review a well-studied controller. In Section III, we describe the approximate abstraction for perception error bounds via sampling from vision-based pose estimation. In Section IV, we show the safe separation under perception error using our main theory of ultimate boundedness. We then validate with AirSim simulation in Section V and conclude in Section VI.

II. VISION-BASED FORMATION CONTROL

We will study a distributed formation control system with N identical aerial vehicles or *agents* as shown in Figure 1. The target formation is specified in terms of relative positions between agents. Each agent i has a downward facing camera, and it uses images from its own camera and its neighbor j 's camera to periodically estimate the relative position of j with respect to i . Based on these estimated relative positions to all its neighbors, agent i then updates its own position by setting a velocity, to try and achieve the target formation.

Before describing the vision and control modules in more detail, we introduce some notations used throughout the paper. First, the neighborhood relation between agents is defined by an $N \times N$ symmetric adjacency matrix W , i.e., j is a neighbor of i if and only if $\omega_{ij} = 1$, otherwise $\omega_{ij} = 0$. All diagonal entries of W are $\omega_{ii} = 0$.

Second, we only consider planar formations for simplicity although the agents are in 3-dimensional space. Thus, the

position of agent i in the world frame is represented by a vector $q_i \in \mathbb{R}^2$ and its input velocity by another vector $u_i \in \mathbb{R}^2$. The state of the overall system is $q = [q_1^T \ q_2^T \ \dots \ q_N^T]^T$. A desired formation is specified as the set of target equilibrium states defined by a desired state q^* :

$$E_{q^*} := \{q \mid \forall i, j \in \{1 \dots N\}, q_j - q_i = q_j^* - q_i^*\}.$$

That is, E_{q^*} is the set of all states that form q^* up to position translations. We also specify a safe set demanding that the distance between any two agents are never too close, namely,

$$S := \{q \mid \forall i, j \in \{1 \dots N\}, \|q_j - q_i\| > 0\}$$

We now discuss the components of an agent i (Figure 2).

A. Vision-based relative pose estimation

Agent i 's downward-facing camera s periodically generates an image of the ground m_i , which depends on its state q_i and other environmental factors like background scenery, lighting, fog, etc. The neighboring agent j generates another image m_j of the ground and shares this with agent i over the communication channel. We assume the whole system runs in synchronous mode, i.e. all the drones will capture the image at the same time and there's no communication delay between drones while sharing the images. The vision-based pose estimation algorithm h takes a pair of images, m_i and m_j , as an input and produces the estimated relative position \hat{q}_{ij} of j with respect to i following these steps:

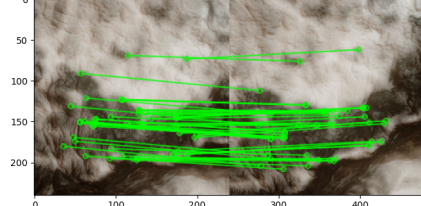


Fig. 3. Feature matching on a pair of images collected in AirSim.

(1) First, h detects features from each image. Any of the various feature detection algorithms like SIFT [15], SURF [16], and ORB [17] can be used for this step. (2) Then, h collects the detected features from the pair of images, and a feature matching algorithm (such as FLANN [18]) is used to match pairs of features in each image as shown in Figure 3. (3) For each feature point, we can setup a relationship between the pixel coordinate and the feature's world coordinate

$$s \begin{bmatrix} u \\ v \\ 1 \end{bmatrix} = K[R \mid t] \begin{bmatrix} x \\ y \\ z \\ 1 \end{bmatrix}$$

where $[u, v, 1]^T$ is the pixel coordinate, $[x, y, z, 1]$ is the feature's world coordinate, K is the camera intrinsic matrix and $[R \mid t]$ is the extrinsic camera parameters. With a set of at least 8 matched features, we can come up with 8 pairs of equations between the pose of two cameras and by solving these

equations, the relative rotation and the normalized translation vector can be calculated using the inverse geometry of image formation in cameras. Examples of this step appear in [19]–[21]. Further, the altitude information and drone orientation can be used to estimate the true distance to ground and recover the length of the translation vector.

The accuracy of the perception pipeline can be influenced by many factors. The change of environments such as background, lighting, and weather influence the quality of the image and the image features, which in turn influence the accuracy of relative pose estimation.

B. Formation control

The relative pose estimates computed by agent i 's perception modules are used to compute its velocity control inputs u_i , which in turn affects its position q_i . We consider the simple single-integrator dynamics relating q_i and u_i :

$$\dot{q}_i = u_i$$

The velocity control input is calculated using the well-known averaging rule [22]:

$$u_i = \sum_{j \in \{1 \dots N\}} \omega_{ij} (\hat{q}_{ij} - q_{ij}^*). \quad (1)$$

where we use the notation $q_{ij} = q_j - q_i$ and $q_{ij}^* = q_j^* - q_i^*$.

In [22], it is proven that this controller stabilizes the system to a desired formation *if there is no perception error*, i.e., $\hat{q}_{ij} = q_{ij}$.

Finally, we study the ultimate boundedness [10] of the system. For the formation control, the ultimate bound is a constant c bounding the relative distance when the system is stabilized. Formally, a state q within the ultimate bound b is that, for each pair of $i, j \in \{1 \dots N\}$

$$\|q_{ij}^* - q_{ij}\| \leq b.$$

III. PIECEWISE APPROXIMATE ABSTRACTION

In this section, we first develop a model of the perception error which will be used later in our safety analysis. For vision-based perception, uniform worst case bounds on the perception error $\hat{q}_{ij} - q_{ij}$ can be overly conservative for system-level analysis. Recent research has shown that state-dependent error models can strike a balance between the conservatism of the safety analysis and the precision of characterizing deep learning-based perception systems [9].

Following the above pattern, we investigate the relationship between the ground truth and the perceived relative poses. We randomly sample pairs of camera images from two drones under different relative positions in AirSim. For each sample, we obtain a pair of true relative position q_{ij} from AirSim and perceived relative position \hat{q}_{ij} via vision-based pose estimation pipeline (of Section II-A). Figure 4 plots the norm of perception error $\|\hat{q}_{ij} - q_{ij}\|$ with respect to the true relative distance $\|q_{ij}\|$. We observe that the norm of the worst-case perception error indeed increases with respect to the true relative distance. Secondly, the error bound grows sharply when the relative distance crosses certain threshold, e.g., about 14 meters in Figure 4. This is not too surprising:

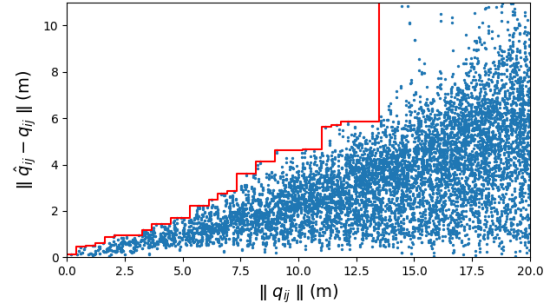


Fig. 4. Perception error distances $\|\hat{q}_{ij} - q_{ij}\|$ (Blue dots) and empirical piecewise constant upper bound (Red line) with respect to true relative distances $\|q_{ij}\|$. We fix drone i as the origin and uniformly sample 10,000 positions of drone j within a circle of 20 meters in the LandscapeMountains environment from AirSim.

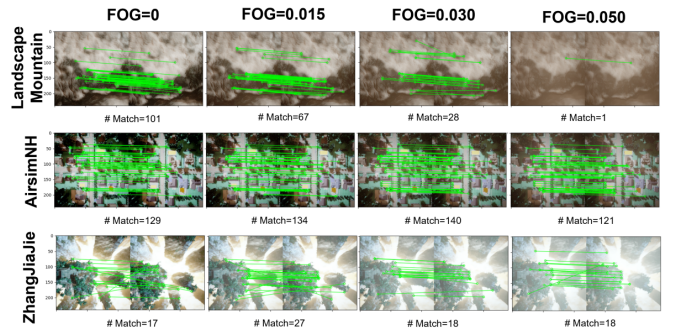


Fig. 5. Matched feature points found by the feature detection and matching algorithm under three AirSim environments and four fog levels.

As the two drones become farther apart, the intersection of the two camera views is smaller, and there are fewer matched features than eight pairs, which leads to the failure of relative pose estimation.

For the analysis later in Section IV, our goal is to find an abstraction of the vision component with its worst perception error, and we empirically approximate the worst perception error from collected samples. Hence, we define the *approximate abstraction* as the piecewise constant function bounding the perception errors² as illustrated by the red line in Figure 4. Formally, given a sequence of $0 < d_1 < d_2 < \dots < d_n$, we find a non-decreasing sequence $\gamma_1 \leq \gamma_2 \leq \dots \leq \gamma_n$, such that γ_k serves as the empirical upper bound on the error for all intervals $(d_{k-1}, d_k]$. We then construct the monotonic piecewise constant function γ_{\max} ,

$$\gamma_{\max}(q_{ij}) = \begin{cases} \gamma_1, & \text{if } 0 \leq \|q_{ij}\| \leq d_1 \\ \vdots \\ \gamma_n, & \text{if } d_{n-1} < \|q_{ij}\| \leq d_n \\ \infty, & \text{if } d_n < \|q_{ij}\| \end{cases} \quad (2)$$

The approximate abstraction will depend on environmental factors. To systematically study the impact of environmental variations on the approximate abstraction, we experimented with different environments and weather conditions in the photorealistic AirSim simulator. Figure 5 shows how the

²Other possible error models could also be investigated. For example, in [9] a piece-wise affine model proved to be effective.

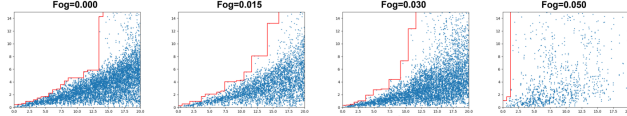


Fig. 6. Perception error distances $\|\hat{q}_{ij} - q_{ij}\|$ and empirical piecewise constant upper bound with respect to true relative distances $\|q_{ij}\|$ under varying fog levels.

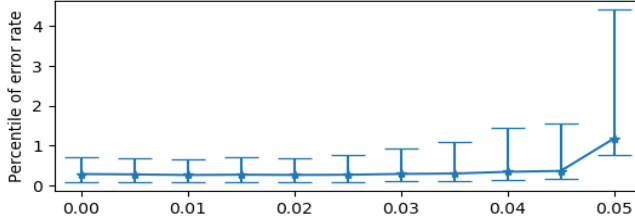


Fig. 7. 25%, 50%, and 75% percentiles on relative perception error $\frac{\|\hat{q}_{ij} - q_{ij}\|}{\|q_{ij}\|}$ with respect to different fog levels under LandscapeMountains.

feature matching step degrades across three environments (namely **LandscapeMountains**, **AirSimNH**, and **ZhangJiajie**) and four fog levels. Note that at the fog level 0.050, only one pair of matching features is detected for **LandscapeMountains** for the same relative position.

Figure 6 shows the approximate abstractions for four fog levels under **LandscapeMountains**. The perception error bound increases much faster (against the relative distance) in a fogger weather. To better visualize this trend, we normalize the perception error, $\|\hat{q}_{ij} - q_{ij}\|$, to the *relative perception error*, $\frac{\|\hat{q}_{ij} - q_{ij}\|}{\|q_{ij}\|}$, and plot the 25%, 50%, and 75% percentiles of relative perception error for more finer fog levels in Figure 7. We observe in Figure 7 that the 50% value (median) mostly remains the same except until fog level is 0.05, but the value of 75% percentile increases more significantly. This is consistent with the observation on the approximate abstraction.

IV. ULTIMATE BOUND ON RELATIVE POSITIONS

The controller in Equation (1) assumes the true relative positions q_{ij} is used. However, we already show in Section III that the estimated relative positions from vision algorithms are imprecise and affected by ground truth and environmental variations. In this section, we first assume that the maximum perception error from vision algorithms are bounded. We show that the true relative positions between agents is ultimately bounded around the desired formations, and the ultimate bound is limited by a constant multiplied to the perception error bound. We further discuss the analysis using the approximate abstraction obtained in Section III.

First, we introduce the graph induced Laplacian matrix, the error dynamics without perception error, and the Lyapunov function for reference in the subsequent proofs. Laplacian matrix L is defined using the adjacency matrix W as:

$$l_{ij} = \begin{cases} \sum_{k \in \{1 \dots N\}} \omega_{ik} & i = j \\ -\omega_{ij} & i \neq j \end{cases}$$

L is symmetric and positive semi-definite for a simple undirected graph. The smallest eigenvalue λ_1 of L is always 0 with the eigenvector $\vec{1} = [1, 1, \dots, 1]^T$. If the graph is connected, then $\text{rank}(L) = N - 1$. Further, the second smallest eigenvalue λ_2 of L is called the *algebraic connectivity* of the interaction graph [23].

Given the error state defined as $e_q = q^* - q$, the error dynamics without perception error is derived as:

$$\dot{e}_q = -Le_q \quad (3)$$

where $L = L \otimes I_2$ is the Kronecker product to extend the Laplacian matrix for 2D positions.

We use the quadratic function V below to prove the Lyapunov stability for the system without perception error and the ultimate boundedness of the system with perception error:

$$V(e_q) = \frac{1}{2} \sum_{i \in \{1 \dots N\}} \sum_{j \in \{1 \dots N\}} \omega_{ij} \|q_{ij} - q_{ij}^*\|^2 = \frac{1}{2} e_q^T L e_q \quad (4)$$

Theorem 1: Assume that the interaction graph is connected and there is no perception error, $\hat{q}_{ij} = q_{ij}$, the state of the system q converges to desired formations E_{q^*} .

Proof: The Lyapunov stability for the controller in [22] is a well-established result (see Chapter 6 in [3] for a detailed proof). In short, the derivative \dot{V} is always non-positive:

$$\dot{V}(e_q) = e_q^T L \dot{e}_q = -e_q^T L^2 e_q = -\|Le_q\|^2 \leq 0$$

This is because L is positive semi-definite. By LaSalle's invariance principle, the error state e_q converges to the null space of L , i.e., the error state e_q converges to eigenvectors in $\text{span}\{\vec{1}\}$. Thus, the system state q converges to E_{q^*} . ■

Now we analyze the system with perception error $\hat{q}_{ij} \neq q_{ij}$ following the analysis steps for ultimate boundedness [10]. We define the perception error as $\gamma_{ij} = \hat{q}_{ij} - q_{ij}$. Further, the perception errors for all pairs of agents is denoted as a $N \times N$ matrix Γ . We now rewrite the controller in Equation (1):

$$u_i = \sum_{j \in \{1 \dots N\}} \omega_{ij} (\hat{q}_{ij} - q_{ij}^*) = \sum_{j \in \{1 \dots N\}} \omega_{ij} (q_{ij} + \gamma_{ij} - q_{ij}^*)$$

Lemma 1: If the algebraic connectivity of the communication graph $\lambda_2 \geq 1$ and all perception errors are bounded $\|\gamma_{ij}\| \leq \gamma_{\max}$, the error state is ultimately bounded by the sub-level set $\{e_q \mid V(e_q) \leq \rho\}$ where

$$\rho = \frac{N}{2} \cdot (N - 1)^2 \cdot \gamma_{\max}^2$$

Proof: Given error state $e_q = q^* - q$, the error dynamics from Equation (3) is modified as:

$$\dot{e}_q = -(Le_q + (W \odot \Gamma)\vec{1})$$

In short, $(W \odot \Gamma)\vec{1}$ represents the perception error induced disturbance. The element-wise multiplication $(W \odot \Gamma)$ states that each pairwise error γ_{ij} is amplified by the weighted edge ω_{ij} . The product of $(W \odot \Gamma)$ and $\vec{1}$ then aggregates the disturbance for agent i from all neighbors j .

We first derive the bound on $\|(W \odot \Gamma)\vec{\mathbf{1}}\|$. By definition,

$$(W \odot \Gamma)\vec{\mathbf{1}} = \begin{bmatrix} 0 & \omega_{12}\gamma_{12} & \dots & \omega_{1N}\gamma_{1N} \\ \omega_{21}\gamma_{21} & 0 & \dots & \omega_{2N}\gamma_{2N} \\ \vdots & \vdots & \ddots & \vdots \\ \omega_{N1}\gamma_{N1} & \omega_{N2}\gamma_{N2} & \dots & 0 \end{bmatrix} \vec{\mathbf{1}} = \begin{bmatrix} \sum_{j \neq 1} \omega_{1j}\gamma_{1j} \\ \vdots \\ \sum_{j \neq N} \omega_{Nj}\gamma_{Nj} \end{bmatrix}$$

Because $\|\gamma_{ij}\| \leq \gamma_{\max}$ and $\omega_{ij} \in \{0, 1\}$, the norm can be bounded by:

$$\|(W \odot \Gamma)\vec{\mathbf{1}}\| = \sqrt{\sum_i (\sum_{j \neq i} \omega_{ij}\gamma_{ij})^2} \leq \sqrt{N((N-1)\gamma_{\max})^2} = \sqrt{2\rho}$$

Because the algebraic connectivity $\lambda_2 \geq 1$, we know $\mathbf{e}_q^T \mathbf{L}^2 \mathbf{e}_q \geq \mathbf{e}_q^T \mathbf{L} \mathbf{e}_q$. Therefore, for $V(\mathbf{e}_q) = \frac{1}{2} \mathbf{e}_q^T \mathbf{L} \mathbf{e}_q > \rho$,

$$\begin{aligned} \mathbf{e}_q^T \mathbf{L}^2 \mathbf{e}_q &\geq \mathbf{e}_q^T \mathbf{L} \mathbf{e}_q > 2\rho \\ \Rightarrow \|\mathbf{L} \mathbf{e}_q\| &> \sqrt{2\rho} \geq \|(W \odot \Gamma)\vec{\mathbf{1}}\| \end{aligned}$$

We then consider \dot{V} :

$$\begin{aligned} \dot{V}(\mathbf{e}_q) &= \mathbf{e}_q^T \mathbf{L} \dot{\mathbf{e}}_q = -\mathbf{e}_q^T \mathbf{L} (\mathbf{L} \mathbf{e}_q + (W \odot \Gamma)\vec{\mathbf{1}}) \\ &= -\|\mathbf{L} \mathbf{e}_q\|^2 - \langle \mathbf{L} \mathbf{e}_q, (W \odot \Gamma)\vec{\mathbf{1}} \rangle \\ &= -\|\mathbf{L} \mathbf{e}_q\|^2 - \|\mathbf{L} \mathbf{e}_q\| \|(W \odot \Gamma)\vec{\mathbf{1}}\| \cos \theta \\ &\leq -\|\mathbf{L} \mathbf{e}_q\|^2 + \|\mathbf{L} \mathbf{e}_q\| \|(W \odot \Gamma)\vec{\mathbf{1}}\| \\ &= -\|\mathbf{L} \mathbf{e}_q\| (\|\mathbf{L} \mathbf{e}_q\| - \|(W \odot \Gamma)\vec{\mathbf{1}}\|) \\ &< 0 \quad \because \|\mathbf{L} \mathbf{e}_q\| > \|(W \odot \Gamma)\vec{\mathbf{1}}\| \geq 0 \end{aligned}$$

where $\langle \cdot, \cdot \rangle$ denotes the inner product of two vectors.

Thus, we know the system will eventually enter the sub-level set $\{\mathbf{e}_q \mid V(\mathbf{e}_q) \leq \rho\}$. \blacksquare

Theorem 2: If the interaction graph is a *complete graph*, the true relative position q_{ij} of each pair of drones is ultimately bounded around the desired relative position q_{ij}^* . Formally, for all i, j ,

$$\|q_{ij} - q_{ij}^*\| \leq b.$$

where $b = \sqrt{\frac{\rho}{N-1}} = \gamma_{\max} \sqrt{\frac{N(N-1)}{2}}$ is the ultimate bound.

Proof: Recall the Lyapunov function at Equation (4). When the system enters the ultimate bound $\{\mathbf{e}_q \mid V(\mathbf{e}_q) \leq \rho\}$,

$$V(\mathbf{e}_q) = \frac{1}{2} \sum_{i \in \{1 \dots N\}} \sum_{j \in \{1 \dots N\}} \omega_{ij} \|q_{ij} - q_{ij}^*\|^2 \leq \rho$$

We can see the sum of square for all $\|q_{ij} - q_{ij}^*\|$ is bounded. Without loss of generality, we assume $\|q_{ij} - q_{ij}^*\| = 0$ for $i \neq 1$ and $j \neq 1$ to find the upper bound on $\|q_{1j} - q_{1j}^*\|$. This implies all drones except drone 1 is in the desired formation up to translation, that is, $(q_2 - q_2^*) = \dots = (q_N - q_N^*) = \Delta q$. We can find for $j \neq 1$

$$\begin{aligned} q_{1j} - q_{1j}^* &= (q_j - q_1) - (q_j^* - q_1^*) = (q_j - q_j^*) - (q_1 - q_1^*) \\ &= \Delta q - (q_1 - q_1^*) \end{aligned}$$

For a complete graph, we can simplify $V(\mathbf{e}_q)$ as

$$\begin{aligned} V(\mathbf{e}_q) &= \frac{1}{2} \left(\sum_{j \neq 1} \|q_{1j} - q_{1j}^*\|^2 + \sum_{i \neq 1} \|q_{ii} - q_{ii}^*\|^2 \right) \\ &= \sum_{j \neq 1} \|q_{1j} - q_{1j}^*\|^2 = \sum_{j \neq 1} \|\Delta q - (q_1 - q_1^*)\|^2 \\ &= (N-1) \|\Delta q - (q_1 - q_1^*)\|^2 \leq \rho \end{aligned}$$

Hence, $\|q_{1j} - q_{1j}^*\| = \|\Delta q - (q_1 - q_1^*)\| \leq \sqrt{\frac{\rho}{N-1}} = b$ \blacksquare

We can use the ultimate bound from Theorem 2 to provide the safety guarantees.

Proposition 1: Given the interaction graphs is a complete graph, all perception errors are bounded $\|\gamma_{ij}\| \leq \gamma_{\max}$, when the system has stabilized to the ultimate bound, the relative distance is both upper and lower bounded. Formally, for all $i, j \in \{1 \dots N\}$ and $i \neq j$

$$\|\gamma_{ij}\| \leq \gamma_{\max} \implies \|q_{ij}^*\| - b \leq \|q_{ij}\| \leq \|q_{ij}^*\| + b.$$

Further, if $\|q_{ij}^*\| > b$, the system stays in the safe set S .

$$\|q_{ij}^*\| > b \implies \|q_{ij}\| > 0$$

Proof: The proof is to apply the triangle inequalities, e.g., for the lower bound, $\|q_{ij}^*\| - \|q_{ij}\| \leq \|q_{ij}^* - q_{ij}\| \leq b$. Dually, we can derive the upper bound. \blacksquare

Finally, the above analysis of the ultimate boundedness assumes a bound γ_{\max} on maximum perception error for the worst case analysis. As a result, this perception error bound and the derived ultimate bound on distance can be overly conservative if we use the global maximum value regardless of the ground truth. To calculate a more practical bound, our main insight is to use a tighter perception error bound around the desired formation where the ultimate boundedness from Theorem 2 holds locally. This ensures that not only the system stays within the neighborhood around the desired formation but also, because it stays in the neighborhood, the perception error is not becoming worse and hence bounded locally at the same time.

Given the desired relative position q_{ij}^* and the approximate abstraction $\gamma_{\max}(q_{ij})$ in Equation (2), we linearly search for a pair of d_k and γ_k from γ_{\max} such that:

$$\|q_{ij}^*\| + \gamma_k \sqrt{\frac{N(N-1)}{2}} \leq d_k$$

If a pair is found, γ_k is the local perception error bound, and $\gamma_k \sqrt{\frac{N(N-1)}{2}}$ is the local ultimate bound on $\|q_{ij}^* - q_{ij}\|$.

Note that we may fail to find any pair of d_k and γ_k from γ_{\max} and fall back to the maximum perception error. A common case is when the desired distance $\|q_{ij}^*\|$ is specified in the range where the perception performs poorly. For instance, we can choose $\|q_{ij}^*\|$ over 14 meters, and it is expected there is no good local bound according to Figure 4.

V. EXPERIMENTS

In our experiments, we aim to validate two claims: (1) The safe separation and formation are ensured by Theorem 2 and Proposition 1. (2) The analysis of ultimate bounds is robust against varying approximate abstractions from different environments.

Experiment Setup: We present the results from two experiment settings with three and four drones. For three drones, the drones will be placed initially in a line with 6m interval between drones and form an equilateral triangle with edge length 5m. For four drones, the drones are placed initially in a line with 4m interval and form a square with edge length 5m. Then, we simulate each formation for 10

runs in environment AirSimNH under different environmental parameters by varying the fog level in the scenario. The approximate abstractions are obtained by random sample pairs of images in each of the environment.

We conduct our experiments on a workstation with Intel Core i7-10700K @ 3.80GHz, 32GB main memory, and Nvidia GTX1080Ti GPU installed with Ubuntu 20.04 LTS, Python 3.8, and OpenCV 4.6.0. We use the Python API for the v1.8.1-Linux version of the AirSim simulator [11].

A. Safety Assured Formation

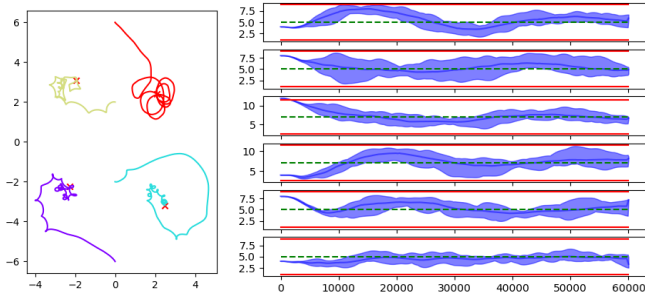


Fig. 8. Absolute position (Left) from one simulation run and relative distance between pairs of drones for 10 simulation runs (Right) for four drones in environment AirSimNH with no fog. For the plot on the left, each color represents the absolute position of a drone. For the plot on the right, each row shows true relative distance $\|q_{ij}\|$ (Blue region), desired distance $\|q_{ij}^*\|$ (Green dashed lines), and derived ultimate bounds for safety and closeness using approximate abstractions (Red lines).

We validate our claim that each pair of drones will maintain a relative distance $\|q_{ij}\|$ around the distance $\|q_{ij}^*\|$ specified for the formation. Figure 8 shows results for four drones formation. The trajectories of drones are on the left, and true relative distances evolving with time for all six pairs of drones are on the right. The trajectories show the drone still attempting to form the desired shapes under perception error. On the right, we see that the true relative distance can get really close to the ultimate bound in several simulation runs. Nevertheless, the system never leaves the ultimate bound, and this is consistent with our analysis that entering the ultimate bound ensures formations and safe separation.

B. Robustness of Ultimate Bound Analysis

In this section, we look at how robust is our analysis across environmental variations. We vary the weather condition by adding different amounts of fog. We experiment with three different fog levels, 0, 0.01, and 0.02, and derive the approximate abstraction from sampled data under each weather condition. We obtain the ultimate bound and repeat the same simulation. The simulated result is shown in Figure 9. We observe that even with the fog introduced, the true relative distance between each pair of drones will still not exceed the ultimate bound derived for the corresponding environment. We also observe that in a foggy environment, where the performance of the vision component worsens, the formation becomes less stable. In the meantime, the ultimate bound becomes more conservative, preventing the relative distance from violating the bound. Note that when the bound becomes

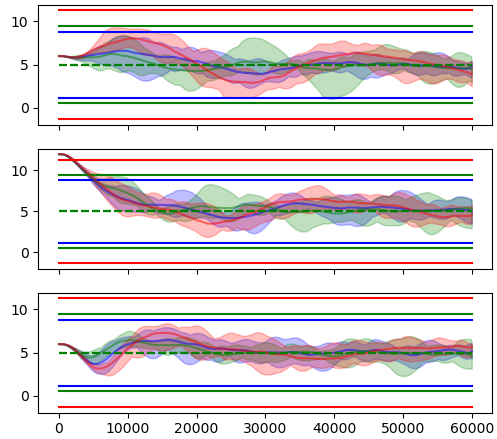


Fig. 9. Relative distance between three pairs of drones for 10 simulation runs under three different levels of fog (level 0 Blue, level 0.01 Green, and level 0.02 Red). The upper and lower bound on distances is not violated with the change of environmental parameters.

larger than the desired relative distance between drones, the lower bound on distances can go below 0. In this case, the premise of Proposition 1 is no longer satisfied, and the drones may actually collide.

VI. LIMITATIONS AND DISCUSSION

We presented an analysis for the safety of a vision-based formation control system. To tackle the vagaries of the perception component, our approach uses an approximate abstraction. This piece-wise constant approximation captures the worst perception error in relative position estimates from the vision component, which is then used to prove that the drones are safely separated and stay close to the desired formation. The analysis uses lower and upper bounds on the distance between agents, and both bounds are derived from the ultimate bound that reuses the Lyapunov-style stability proof. We also systematically studied the impact of environmental variations on the approximate abstraction. Our evaluation with AirSim simulator validates the guarantee on safe separation while achieving formations. We show that the analysis is robust across different environmental variations.

Our study assumed that all drones run synchronously and exchange image feature descriptors instantly. This is obviously an idealization. Our analysis will work without this assumption by bounding the change in relative positions. Under a fixed communication delay, the change in relative positions can be bounded and modeled as part of the perception error.

The study suggests several future directions. First, our current analysis does not provide any guarantee on the time of convergence to the ultimate bound. One direction is to view our approximate abstraction, the piece-wise constant function, as the quantization of the perception output. Existing analysis on quantized consensus algorithms may provide the convergence rate [24]. Another direction is to explore the latest result on ultimate boundedness for state dependent disturbances [25].

REFERENCES

[1] V. Blondel, J. Hendrickx, A. Olshevsky, and J. Tsitsiklis, “Convergence in multiagent coordination consensus and flocking,” in *Proceedings of the Joint forty-fourth IEEE Conference on Decision and Control and European Control Conference*, 2005, pp. 2996–3000.

[2] R. Saber and R. Murray, “Flocking with obstacle avoidance: cooperation with limited communication in mobile networks,” in *42nd IEEE International Conference on Decision and Control (IEEE Cat. No.03CH37475)*, vol. 2, 2003, pp. 2022–2028 Vol.2.

[3] M. Mesbahi and M. Egerstedt, *Graph Theoretic Methods in Multiagent Networks*. Princeton: Princeton University Press, 2010.

[4] F. Bullo, J. Cortés, and S. Martínez, *Distributed Control of Robotic Networks: A Mathematical Approach to Motion Coordination Algorithms*. Princeton University Press, 2009.

[5] E. Montijano, E. Cristofalo, D. Zhou, M. Schwager, and C. Sagüés, “Vision-Based Distributed Formation Control Without an External Positioning System,” *IEEE Transactions on Robotics*, vol. 32, no. 2, pp. 339–351, 2016.

[6] K. Fathian, E. Doucette, J. W. Curtis, and N. R. Gans, “Vision-based distributed formation control of unmanned aerial vehicles,” 2018.

[7] M. M. H. Fallah, F. Janabi-Sharifi, S. Sajjadi, and M. Mehrandezh, “A visual predictive control framework for robust and constrained multi-agent formation control,” *J. Intell. Robotics Syst.*, vol. 105, no. 4, aug 2022.

[8] M. Abraham, A. Mayne, T. Perez, I. Oliveira, H. Yu, C. Hsieh, Y. Li, D. Sun, and S. Mitra, “Challenges in rebooting autonomy with deep learned perception,” in *To Appear in EMSOFT 2022*, 2022.

[9] C. Hsieh, Y. Li, D. Sun, K. Joshi, S. Misailovic, and S. Mitra, “Verifying Controllers with Vision-based Perception Using Safe Approximate Abstractions,” *IEEE Transactions on Computer-Aided Design of Integrated Circuits and Systems*, 2022.

[10] G. Leitmann, “Guaranteed ultimate boundedness for a class of uncertain linear dynamical systems,” *IEEE Transactions on Automatic Control*, vol. 23, no. 6, pp. 1109–1110, 1978.

[11] S. Shah, D. Dey, C. Lovett, and A. Kapoor, “AirSim: High-Fidelity Visual and Physical Simulation for Autonomous Vehicles,” in *Field and Service Robotics*, M. Hutter and R. Siegwart, Eds. Cham: Springer International Publishing, 2018, pp. 621–635.

[12] T. Dreossi, D. J. Fremont, S. Ghosh, E. Kim, H. Ravanbakhsh, M. Vazquez-Chanlatte, and S. A. Seshia, “VerifAI: A Toolkit for the Formal Design and Analysis of Artificial Intelligence-Based Systems,” in *Proc. 31st Int. Conf. Computer Aided Verification*, 2019, pp. 432–442.

[13] S. M. Katz, A. L. Corso, C. A. Strong, and M. J. Kochenderfer, “Verification of image-based neural network controllers using generative models,” *Journal of Aerospace Information Systems*, vol. 19, no. 9, pp. 574–584, 2022.

[14] U. Santa Cruz and Y. Shoukry, “NNLander-VeriF: A Neural Network Formal Verification Framework for Vision-Based Autonomous Aircraft Landing,” in *NASA Formal Methods*, J. V. Deshmukh, K. Havelund, and I. Perez, Eds. Cham: Springer International Publishing, 2022, pp. 213–230.

[15] D. G. Lowe, “Distinctive Image Features from Scale-Invariant Keypoints,” *Int. J. Comput. Vis.*, vol. 60, no. 2, pp. 91–110, 2004.

[16] H. Bay, T. Tuytelaars, and L. Van Gool, “SURF: Speeded Up Robust Features,” in *Computer Vision – ECCV 2006*, A. Leonardis, H. Bischof, and A. Pinz, Eds. Berlin, Heidelberg: Springer Berlin Heidelberg, 2006, pp. 404–417.

[17] E. Rublee, V. Rabaud, K. Konolige, and G. Bradski, “ORB: An efficient alternative to SIFT or SURF,” in *2011 International Conference on Computer Vision*, Nov. 2011, pp. 2564–2571.

[18] M. Muja and D. G. Lowe, “Fast Approximate Nearest Neighbors with Automatic Algorithm Configuration,” in *VISAPP 2009 - Proc. 4th Int. Conf. Computer Vision Theory and Applications, Lisboa, Portugal, February 5-8, 2009 - Volume 1*, A. Ranchordas and H. Araújo, Eds. INSTICC Press, 2009, pp. 331–340.

[19] E. Malis and M. Vargas, “Deeper understanding of the homography decomposition for vision-based control,” INRIA, Research Report RR-6303, 2007. [Online]. Available: <https://hal.inria.fr/inria-00174036>

[20] D. Nister, “An efficient solution to the five-point relative pose problem,” *IEEE Transactions on Pattern Analysis and Machine Intelligence*, vol. 26, no. 6, pp. 756–770, 2004.

[21] H. Li and R. Hartley, “Five-Point Motion Estimation Made Easy,” in *18th Int. Conf. Pattern Recognition (ICPR’06)*, vol. 1, 2006, pp. 630–633.

[22] D. V. Dimarogonas and K. J. Kyriakopoulos, “A connection between formation infeasibility and velocity alignment in kinematic multi-agent systems,” *Automatica*, vol. 44, no. 10, pp. 2648–2654, 2008.

[23] M. Fiedler, “Algebraic connectivity of graphs,” *Czechoslovak Mathematical Journal*, vol. 23, no. 2, pp. 298–305, 1973. [Online]. Available: <http://eudml.org/doc/12723>

[24] A. Kashyap, T. Başar, and R. Srikant, “Quantized consensus,” *Automatica*, vol. 43, no. 7, pp. 1192–1203, 2007.

[25] S. Olaru and H. Ito, “Characterization of ultimate bounds for systems with state-dependent disturbances,” *IEEE Control Systems Letters*, vol. 2, no. 4, pp. 797–802, 2018.